Structure
Article

Recognition Pliability Is Coupled to Structural Heterogeneity: A Calmodulin Intrinsically Disordered Binding Region Complex

Malini Nagulapalli,[1] Giacomo Parigi,[1] Jing Yuan,[1] Joerg Gsponer,[2,3] George Deraos,[4] Vladimir V. Bamm,[5] George Harauz,[5] John Matsoukas,[4] Maurits R.R. de Planque,[6] Ioannis P. Gerothanassis,[7] M. Madan Babu,[2] Claudio Luchinat,[1,*] and Andreas G. Tzakos[7,*]

[1]Magnetic Resonance Center (CERM), University of Florence, Via Luigi Sacconi 6, 50019 Sesto Fiorentino, Italy
[2]MRC Laboratory of Molecular Biology, Cambridge CB2 0QH, UK
[3]Centre for High-Throughput Biology, University of British Columbia, Vancouver, British Columbia V6T 1Z4, Canada
[4]Department of Chemistry, University of Patras, 26500 Patras, Greece
[5]Department of Molecular and Cellular Biology, and Biophysics Interdepartmental Group, University of Guelph, 50 Stone Road East, Guelph, Ontario N1G 2W1, Canada
[6]School of Electronics and Computer Science, University of Southampton, Southampton SO17 1BJ, UK
[7]Department of Chemistry, University of Ioannina, 45110 Ioannina, Greece
*Correspondence: luchinat@cerm.unifi.it (C.L.), atzakos@cc.uoi.gr (A.G.T.)
DOI 10.1016/j.str.2012.01.021

SUMMARY

Protein interactions within regulatory networks should adapt in a spatiotemporal-dependent dynamic environment, in order to process and respond to diverse and versatile cellular signals. However, the principles governing recognition pliability in protein complexes are not well understood. We have investigated a region of the intrinsically disordered protein myelin basic protein ($MBP_{145–165}$) that interacts with calmodulin, but that also promiscuously binds other biomolecules (membranes, modifying enzymes). To characterize this interaction, we implemented an NMR spectroscopic approach that calculates, for each conformation of the complex, the maximum occurrence based on recorded pseudocontact shifts and residual dipolar couplings. We found that the $MBP_{145–165}$-calmodulin interaction is characterized by structural heterogeneity. Quantitative comparative analysis indicated that distinct conformational landscapes of structural heterogeneity are sampled for different calmodulin-target complexes. Such structural heterogeneity in protein complexes could potentially explain the way that transient and promiscuous protein interactions are optimized and tuned in complex regulatory networks.

INTRODUCTION

The myelin sheath has a dynamic structure that enables rapid signal propagation in the nervous system. This dynamic nature can be envisaged as the continuous formation and disruption of interactions in its protein content (Tarassov et al., 2008). To this malleable interaction network (Tarassov et al., 2008), the role of intrinsically disordered proteins (IDPs) (Dunker et al., 2008; Gsponer et al., 2008; Turoverov et al., 2010), protein dynamism (Mittag et al., 2010; Tokuriki and Tawfik, 2009; Tompa and Fuxreiter, 2008), and polymorphic or fuzzy protein complexes (disorder in the bound state) (Tompa and Fuxreiter, 2008) could be crucial in signal fidelity (Gsponer et al., 2008), providing the required complexity and promiscuity for fruitful integration of signal diversity. In a dynamic system the existence of overlapping binding sites (i.e., the same protein region can participate in interactions with multiple protein partners) could provide an additional dimension of functionality-complexity, in the same way that the cell uses standard building blocks to build functionality through combinatorial assembly.

Regions within IDPs employ an intriguing ability to undergo disorder-to-order transitions upon binding in order to perform their function (Dyson and Wright, 2002; Receveur-Bréchot et al., 2006). Although there are several cases of IDPs that have been identified to bind to multiple partners via their ability to adopt distinct conformations (Oldfield et al., 2008), the existence of IDPs that retain their disordered state in the complex should also be investigated. Different recognition binding mechanisms have been suggested for IDPs, and it was recently shown that there is an ensemble of transient intermediate states in the frame of the coupled binding and folded process (Sugase et al., 2007). But we know little about the dynamics, and the structural heterogeneity and ordered/disordered states, of such complexes. If the resulting complexes are conceptualized as static entities, a number of questions emerge. How can multiple and diverse signals in complex dynamic systems, such as myelin, be controlled, monitored, and processed solely via static interactions? A hypothesis is that some degree of heterogeneity must exist also in such complexes to allow signals to be transmitted under evolving environments (Boehr et al., 2009; Csermely et al., 2010, 2011). Indeed, there is an increasing number of cases of disordered complexes appearing, that until recently were largely overlooked (Fong et al., 2009; Mittag et al., 2010; Tokuriki and Tawfik, 2009; Tompa and Fuxreiter, 2008). Therefore, the questions that emerge are how much intrinsic disorder exists in such complexes,

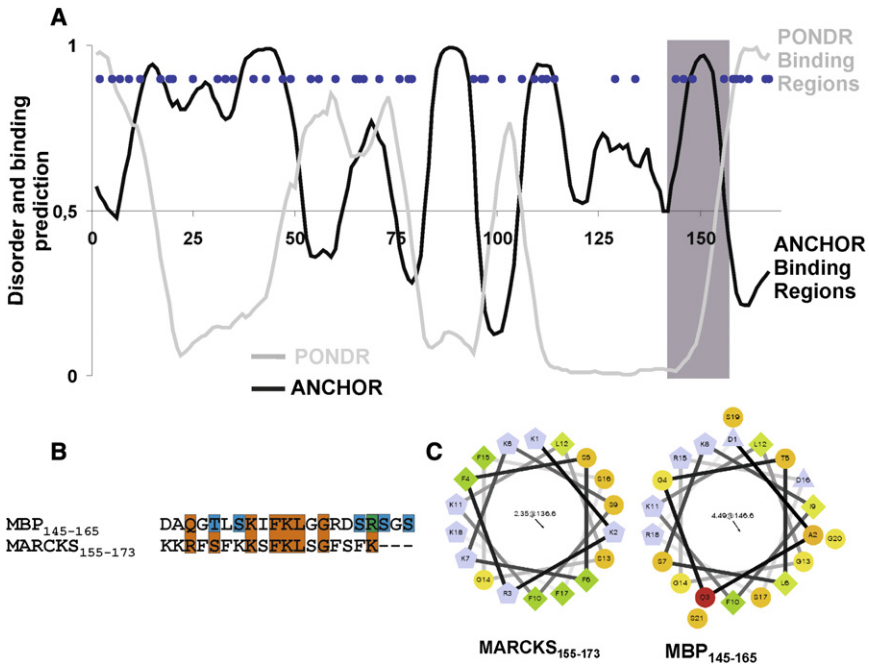

Figure 1. Disordered and Binding Regions in MBP and Comparison to MARCKS Protein

(A) The gray and black lines denote the degree of intrinsic disorder of MBP predicted by the PONDR (VL-XT Predictor) (Romero et al., 2001) and ANCHOR (Mészáros et al., 2009), respectively. PONDR segments with scores above 0.5 correspond to disordered regions, whereas the reverse stands for ANCHOR predictions. The interaction sites predicted by PONDR and ANCHOR are signaled in the plot by downward spikes (scores below 0.5) and upward spikes (scores above 0.5), respectively. Residues that can be posttranslationally modified in MBP are indicated with blue circles. The gray bar shows the 145–165 segment of human 18.5 kDa MBP ($MBP_{145–165}$) that is predicted to be a consensus disordered binding site by PONDR (black line) and ANCHOR (gray line).

(B) Sequence alignment between the region 145–165 of MBP ($MBP_{145–165}$) and 155–173 of MARCKS ($MARCKS_{155–173}$). Residue homology is depicted with orange bars. Residues that can be posttranslationally modified are also indicated: blue bars, phosphorylation (S and T), site highlighted in green, citrullination (arginine deimination).

(C) Helical wheel representation of $MBP_{145–165}$ and $MARCKS_{155–173}$. Hydrophilic residues are presented as circles (colored in orange or red), hydrophobic residues as diamonds (colored in green), potentially negatively charged as triangles, and potentially positively charged as pentagons.

and what is the conformational space sampled by these complexes.

Myelin basic protein (MBP) is a predominant protein in the multilamellar arrangement of the myelin sheath in the central nervous system (Harauz and Libich, 2009). Consistent with its intrinsically disordered nature, MBP contains numerous posttranslational modification sites and interacts with a wide variety of proteins, including cytoskeletal proteins (Harauz and Libich, 2009) (Figures 1A and 1B). The inherent flexibility of MBP provides a pliable interface that ensues in its centrality in signaling and regulatory networks. However, the centrality of IDPs is often associated with disease due to the high possibility of disruption of the protein interaction network after targeted attacks/modifications to such hubs (Uversky et al., 2008). This could be also the case for MBP, which has been implicated in the demyelinating disease multiple sclerosis (Harauz and Libich, 2009).

The diverse functional characteristics of MBP often involve the entire protein, but the existence of isolated and/or overlapping disordered binding sites is suggested by various studies (Libich et al., 2010). The importance of intrinsically disordered regions in druggable interactions has recently attracted considerable attention (Cheng et al., 2006; Hammoudeh et al., 2009; Metallo, 2010), and novel methods and strategies are required to exploit binding sites within disordered regions (Cheng et al., 2006; Mészáros et al., 2009). Our recent work has also indicated that synthetic linear and circular analogs of specific regions of MBP could potentially form the basis for therapeutic approaches against multiple sclerosis (Tzakos et al., 2004; Deraos et al., 2008; Katsara et al., 2009; Matsoukas et al., 2005).

Here, we focused on an intrinsically disordered secondary immunodominant epitope of MBP ($MBP_{145–165}$) (Sospedra and Martin, 2005) that is susceptible to posttranslational modifications and characterized by recognition promiscuity due to its implication in the binding of cytoskeletal and other cytosolic proteins to a membrane surface (Homchaudhuri et al., 2010). Importantly, it has been mentioned that these associations are modulated by interactions of MBP with calcium(II) bound calmodulin (CaM) (Boggs et al., 2011). Such multifunctionality could suggest the presence of heterogeneity in the relevant complexes, allowing the relevant recognition plasticity to take place. To probe the potential heterogeneous nature of the CaM-$MBP_{145–165}$ complex, we used primarily solution NMR spectroscopy, complemented by several other biophysical techniques.

CaM is a protein composed of two domains (the N-terminal and C-terminal domains), each of them being able to bind two calcium(II) ions. These domains can be considered rigid in the metal bound form (at least as far as the backbone is concerned), but they are quite free to move with respect to one another (Baber et al., 2001; Barbato et al., 1992; Bertini et al., 2004, 2007, 2010). Selective substitution of the calcium(II) ion in the second binding loop of the N-terminal domain in a N60D mutant of CaM with paramagnetic lanthanide(III) ions allowed the measurement of interdomain NMR pseudocontact shifts (pcss) and self-orientation residual dipolar couplings (rdcs). After calculation for each possible conformation of the CaM-$MBP_{145–165}$ complex, the largest maximum occurrence (MO, i.e., the maximum percentage of time that a conformer of a macromolecule can exist) (Bertini et al., 2010), consistent with the recorded pcss and rdcs, we found that the relevant complex was characterized by structural heterogeneity. We then performed a quantitative global comparative analysis of heterogeneity

induced in CaM upon interaction with different targets (Death-associated Protein Kinase [DAPk] [Bertini et al., 2009], α-synuclein [Bertini et al., 2007], $MBP_{145–165}$ as also the free CaM [Bertini et al., 2007, 2010]), and we found that CaM samples different conformations with a characteristic spatial heterogeneity for each case. We propose that this recorded differential heterogeneity could be an important aspect for tuning recognition promiscuity and functionality/malfunctioning at the protein-complex level, and could partially explain how transient and promiscuous protein interactions are optimized and tuned in complex regulatory networks.

RESULTS AND DISCUSSION

A Disordered Noncanonical CaM-Binding Region Located at the C Terminus of MBP

CaM-binding sites in the MBP sequence had been defined by former studies (Libich et al., 2003a, 2003b; Majava et al., 2008, 2010). For instance the interaction of MBP with Ca_4CaM has previously been indicated to involve primarily the C terminus of MBP (Libich and Harauz, 2008; Majava et al., 2008), but other binding sites cannot be excluded (Libich et al., 2003a, 2003b; Majava et al., 2010; Polverini et al., 2004). Indeed, in accordance with these findings, a predictor of CaM-binding regions developed by Radivojac et al. (2006) indicated the presence of two CaM-binding regions in the sequence of MBP, located in the N and C terminus. Recent literature studies have demonstrated not only the diversity of conformations that CaM is able to adopt in accommodating different binding partners but also that novel target sequences exist (Juranic et al., 2010; Samal et al., 2011) and are substantially different from all known CaM-binding domains (Rhoads and Friedberg, 1997). Therefore, the presence of MBP regions that do not resemble canonical CaM-binding motifs should also be investigated (Hoeflich and Ikura, 2002; Ishida and Vogel, 2006). On the basis of recently established algorithms that allow prediction of disordered binding regions in proteins (Mészáros et al., 2009; Romero et al., 2001), it will be important to screen the MBP sequence for such regions that could be implicated in recognition pliability. The prediction of specific binding regions undergoing a disorder-to-order transition (disordered binding regions) using PONDR Predictor (Romero et al., 2001) located a binding site at the C terminus of the 18.5 kDa isoform of MBP (residues 145–165 in the 170 residue human protein) that overlaps with a region that is susceptible to posttranslational modifications (citrullination, serine, and threonine phosphorylation) (Figure 1B) (Harauz and Libich, 2009). The same site was also predicted by another predictor (Mészáros et al., 2009) (Figure 1A). Interestingly, $MBP_{145–165}$ is similar in many respects to the CaM-binding, disordered region of myristoylated alanine-rich C-kinase substrate ($MARCKS_{155–173}$) (Ishiyama et al., 2001) (Figure 1B). Both $MARCKS_{155–173}$ and $MBP_{145–165}$ are predicted to form an amphipathic α helix with the positively charged residues localized on one side of the helix, and the residues altered by post-translational modifications on the opposite side (Figure 1C). The short-sequence motif FKL that is essential to the tight binding of $MARCKS_{155–173}$ to CaM is also present in MBP (Yamauchi et al., 2003). However, of the two lysines (Lys162 and Lys163) in $MARCKS_{155–173}$ that contribute to the stability of the $MARCKS_{155–173}$-CaM complex via the formation of salt bridges with glutamic acids in the two CaM domains, only the one interacting with the C-terminal domain (K152) is present in the MBP sequence (Figure 1B). Such a difference could potentially lead to a more open conformation of a potential $MBP_{145–165}$-CaM complex. Overall, the similarities in the sequence of these two proteins suggest that the $MBP_{145–165}$ region, similar to the $MARCKS_{155–173}$ region (Ishiyama et al., 2001), might bind acidic lipids with high affinity and/or contain a CaM-binding site. On the basis of this recognition pliability, critical questions arise. For instance if this binding region is masked by CaM, how can modifying enzymes access MBP, and how does CaM binding modulate MBP association to the membrane? Could we face the existence of a fuzzy protein complex (Tompa and Fuxreiter, 2008)?

The $MBP_{145–165}$ peptide was synthesized to identify whether this segment would behave similarly to the $MARCKS_{155–173}$ homolog. We employed circular dichroism (CD) spectroscopy to probe the secondary structure of $MBP_{145–165}$ in a lipid environment and its association with model membranes using either pure DMPC or a 3:1 molar DMPC/DMPG mixture (Figure 2A). In the presence of DMPC vesicles (net uncharged yet zwitterionic membrane surface), $MBP_{145–165}$ is characterized by a far-UV CD spectrum typical of an essentially unfolded polypeptide chain (CD spectrum as in 100% water; see Figure S1 available online). With DMPC-DMPG vesicles (net negatively charged membrane surface), the CD spectrum was indicative of an increased α-helical character (CD spectrum as in 80%–100% TFE, Figure S1). This result strongly suggests that the peptide is in the aqueous phase in the DMPC system (weak interaction with the membrane), and undergoes a structural change due to stronger association with the membrane surface in the DMPC-DMPG system. This structural transition is in accordance with the formation of a membrane surface-associated amphipathic α helix (Figure 1C). The CD spectra of the aligned DMPC-DMPG membranes rule out a transmembrane orientation of this region of MBP, in accordance with a solid-state NMR and EPR studies of full-length MBP reconstituted with artificial membranes (Zhong et al., 2007).

Although MBP binds to the membrane, it has been shown that this association is regulated via CaM interaction (Boggs, 2006; Boggs and Rangaraj, 2000; Harauz and Libich, 2009). Here, the Ca_4CaM-$MBP_{145–165}$ interaction has been studied by solution NMR spectroscopy and isothermal titration calorimetry (ITC). The raw ITC data are shown in the upper panel of Figure 2B, and the integrated areas under each peak as a function of the molar ratio of $MBP_{145–165}$ to Ca_4CaM are plotted in the lower panel. Interestingly, the binding curve could be best fitted to a mathematical model describing sequential binding to three sets of binding sites (the parameters of binding are summarized in Table S3). The binding site with the highest affinity to the MBP peptide is characterized by a dissociation constant (K_D) of 8.3 ± 0.1 μM, which is in good agreement with the one calculated from NMR spectroscopy (see below and Figure S2). The affinities of the other two sites do not differ dramatically, being 11.8 ± 0.7 μM and 10.4 ± 0.1 μM, respectively. One potential explanation for this phenomenon could be a "fuzziness" of the Ca_4CaM-$MBP_{145–165}$ complex portraying different conformations of Ca_4CaM or MBP peptide (or both) upon their interaction.

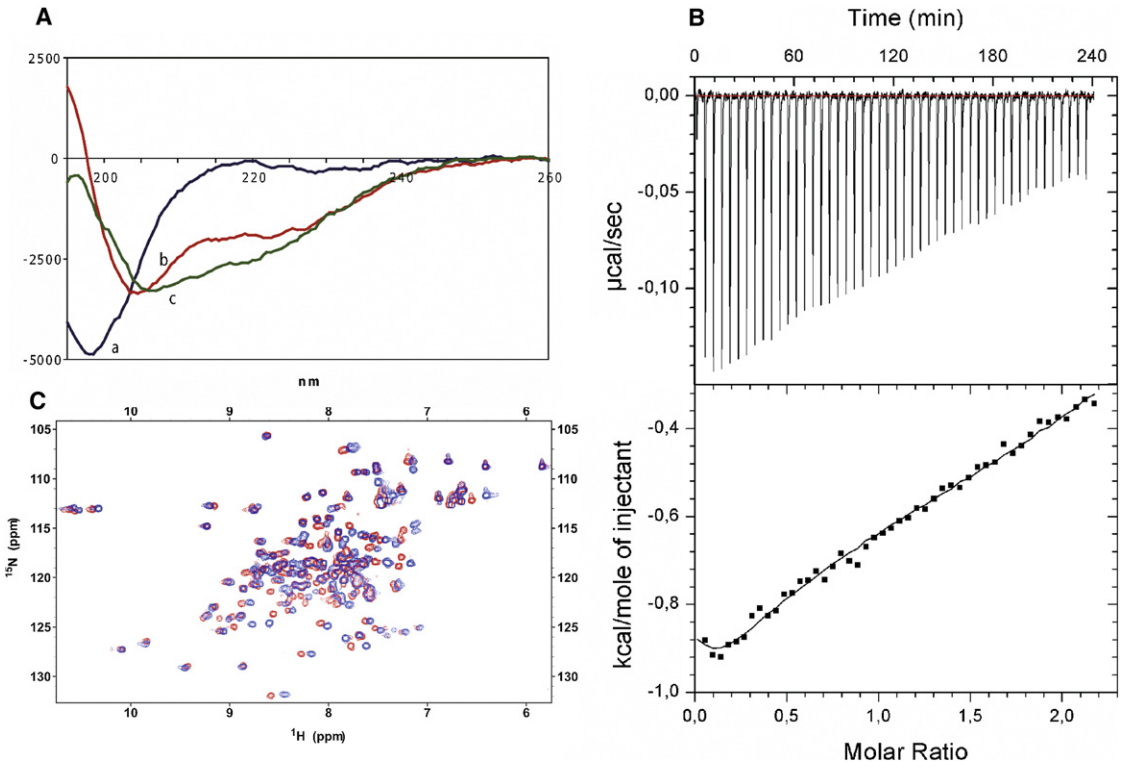

Figure 2. Secondary Structure of $MBP_{145–165}$ and Interactions with CaM

(A) CD spectra of $MBP_{145–165}$ in model membranes: DMPC vesicles (a), DMPC-DMPG vesicles (b), and aligned multilayers of DMPC-DMPG (c).

(B) ITC of Ca_4CaM with $MBP_{145–165}$. The upper panel shows raw data of heat effect (in $\mu cal \cdot s^{-1}$) of 6 µl injections of 1 mM $MBP_{145–165}$ into 1.5 ml of 100 µM Ca_4CaM performed at 300 s intervals. The lower panel shows the fitted binding isotherms. The data points were obtained by integration of heat signals plotted against the molar ratio of $MBP_{145–165}$ to Ca_4CaM in the reaction cell. K_D for the binding site with the highest affinity was determined to be 8.3 µM, and overall K_D was 10.09 µM. The solid line represents a calculated curve using the best-fit parameters obtained by a nonlinear least-squares fit.

(C) ^1H-^{15}N HSQC spectra of Ca_4CaM (red) and Ca_4CaM:$MBP_{145–165}$ = 1:2.25 (blue).

See also Figures S1 and S2, and Tables S3 and S4.

A similar phenomenon was recently described in the binding of Cu^{2+} to αA-crystallin (Singh et al., 2009), where the recorded isotherm could be best fitted into a sequential mode of binding with five sets of binding sites. Assuming that all three sets of binding sites used to fit the ITC isotherm were a consequence of the same site, sampling slightly different structures, the overall K_D of the interaction (expressed as $K_D = [1/(K_{a1} \times K_{a2} \times K_{a3})^{1/3}]$) was calculated to be 10.09 µM. Similar results were also obtained (overall K_D of 16.56 µM) by performing the ITC with the N60D CaM variant Ca_3TmCaM (Figure S2; Table S4). The binding of Ca_4CaM to $MBP_{145–165}$ was additionally monitored by following the changes in the ^1H-^{15}N HSQC spectrum of ^{15}N-labeled Ca_4CaM (Figure 2C). The chemical shifts of the peaks change progressively with increasing the concentration of $MBP_{145–165}$ up to slightly above one equivalent of the peptide, as expected for a system in fast exchange. The chemical shift perturbation between free Ca_4CaM and in the presence of 2.25 equivalents of $MBP_{145–165}$ peptide is shown in Figure 3A. The plot indicates that the residues for which chemical shifts differ most in the two forms are located mainly in the C-terminal domain of CaM (Figure 3B), analogously to other CaM complexes (Abraham et al., 2009; Elshorst et al., 1999; Rodríguez-Castañeda et al., 2010).

From the titration a K_D of 10 µM was estimated (Figure S2) for the Ca_4CaM-$MBP_{145–165}$ interaction, which is in consensus with the relevant value obtained from ITC (Figure S2). This value is also in agreement with the one obtained on the full-length MBP (Libich et al., 2003b).

Heterogeneity and Dynamism in the $MBP_{145–165}$-CaM Complex

Recognition of targets by CaM often results in the reorientation of the N- and C-terminal domains of CaM in a "closed" conformation, i.e., CaM wraps around its target to form a rigid complex. If this is also the case for the molecular recognition of MBP by CaM, then critical concerns could arise on the recognition pliability of the MBP epitope mentioned above. In order to understand how specificity and recognition pliability for different targets is achieved by MBP, we focused on the CaM-$MBP_{145–165}$ recognition mode. Interestingly, in the ITC measurements on the CaM-$MBP_{145–165}$ interaction, the recorded isotherm could be best fitted in a sequential mode of binding having three sets of binding sites, with the binding affinity being in the range 11.8 ± 0.7 µM to 8.3 ± 0.1 µM. This could be an indication that the CaM-$MBP_{145–165}$ interaction might sample different conformations (Singh et al., 2009). We, therefore, explored the

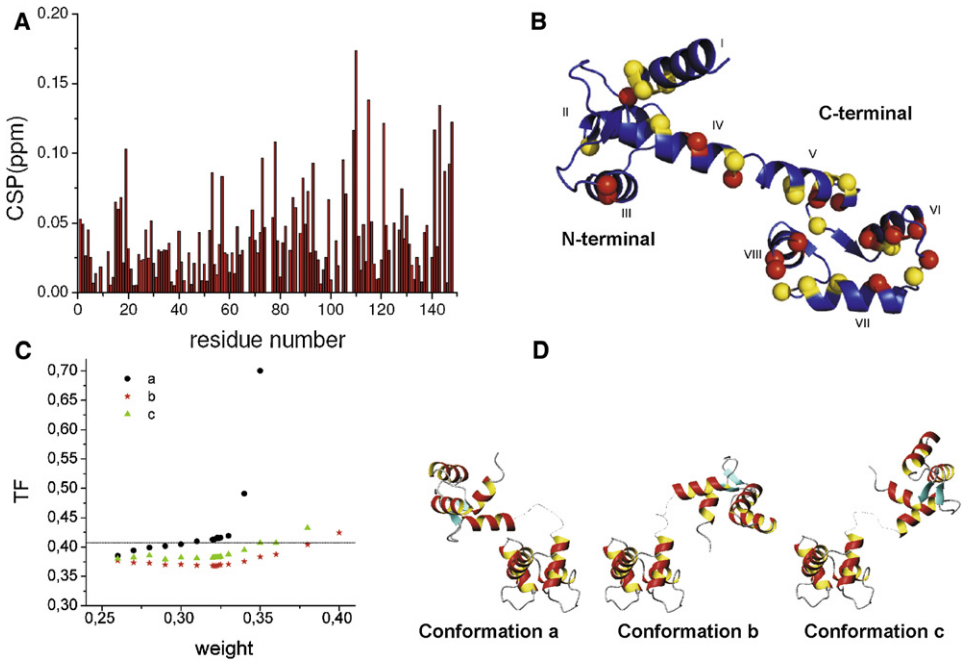

Figure 3. CaM Conformational Responses upon $MBP_{145–165}$ Binding

(A) Composite chemical shift perturbation (CSP) of Ca_4CaM upon peptide binding. The latter was calculated with the equation $CSP = \sqrt{\Delta\delta H^2 + (\Delta\delta N/5)^2}/2$, where $\Delta\delta_H$ and $\Delta\delta_N$ are the differences in the chemical shift of the amide proton and of the nitrogen, respectively.

(B) Residues with $\Delta\delta$ values greater than 0.05 or 0.075 ppm are shown on the CaM structure (in yellow or red, respectively) in the extended conformation observed in the solid state (1CLL).

(C) TF calculated using pcs and rdc data (Equation 3) for the three conformations corresponding to minima around the three relative orientations with largest MO. The MO value for each conformation is defined as the maximum weight corresponding to a TF value equal to 10% increase of the lowest TF (dotted line). The substantial differences in the weight at which the TF value starts increasing thus result in markedly different MO.

(D) The three conformations "a," "b," and "c" with largest MO are shown.

See also Tables S1 and S2, and Figures S3, S4, and S5.

conformational space sampled by domain reorientations in CaM upon MBP epitope binding by using an approach based on the exploitation of rdcs and pcss (Bertini et al., 2002, 2005, 2010), after substitution of a paramagnetic lanthanide ion for one diamagnetic calcium ion of the N60D CaM variant (Bertini et al., 2003, 2004, 2007). It has already been shown that Ln substitution does not affect the protein structure besides the metal coordination sphere (Bertini et al., 2003, 2004, 2007, 2010), and the substitution of the tripositive Ln^{3+} ion for the Ca^{2+} ion is compensated by the additional negative charge introduced by the N60D mutation. This approach involves calculating for each protein conformation the MO consistent with the collected pcs and rdc data, and studying the conformations with the largest MO (Bertini et al., 2007, 2010). The MO of a given conformation is defined as the percentage of time that the system can spend in that conformation that can reproduce the experimental data.

The pcs and rdc values were measured for $(CaX)_N(Ca_2)_C$CaM, with X = Tb, Tm, and Dy (see Supplemental Experimental Procedures; Figures S3 and S4). The magnetic susceptibility anisotropy tensors of the three lanthanides (reported in Table 1), derived from the pcs of the N-terminal domain amide protons of CaM, were found to be in good agreement with values measured previously in different CaM systems (Bertini et al., 2003, 2007, 2009). The rdc values measured for the C-terminal domain of CaM span a much smaller range than that relative to the N-terminal domain, as predicted by the tensors obtained from the pcs of the N-terminal domain of the protein. Such rdc values are different from those previously obtained for the free protein, and also from the values predicted in the absence of conformational freedom, thus indicating that $MBP_{145–165}$ affects the CaM protein conformational ensemble (Figure S4). The mean tensor parameters for the three lanthanides were calculated from the ^{H}H-N rdc of the C-terminal domain of CaM and are reported in Table 1. The axial and rhombic anisotropy values of these tensors are notably much smaller than the corresponding values obtained from the tensors derived from the pcs values of the N-terminal domain, and in some cases also the sign is different. This observation indicates that there is considerable motional averaging. The agreement of so many rdc values in the C-terminal domain with a unique tensor for each metal (Figure S3) indicates that the whole domain moves rigidly with respect to the N-terminal domain. No agreement of the pcs and rdc data could be obtained for any relative position of the two domains (Figure S5).

The magnetic susceptibility anisotropy tensors obtained from N-terminal domain pcs values, and the mean tensors obtained from C-terminal domain rdc values, were first used to calculate the MOs that any orientation of the C-terminal domain of CaM has with respect to the N-terminal domain orientation. This

Table 1. Magnetic Susceptibility Anisotropies of the Different Lanthanides in CaM-MBP

From N-Terminal Domain pcs			
	Tb^{3+}	Tm^{3+}	Dy^{3+}
$\Delta\chi_{ax}$ (10^{-32} m^3)	36.8	26.7	−37.0
$\Delta\ \chi_{rh}$ (10^{-32} m^3)	−16.9	−12.6	−20.2
Euler angles (rad)[a]	2.537, 0.753, −0.650	−1.553, −0.967, −0.625	0.346, −2.540, −0.324
From C-Terminal Domain rdc			
$\Delta\chi_{ax}$ (10^{-32} m^3)	−3.93	1.61	−1.71
$\Delta\ \chi_{rh}$ (10^{-32} m^3)	−2.26	0.65	−0.83
Euler angles (rad)[a]	−2.933, 2.523, 0.277	−0.279, 0.324, −0.828	1.228, 0.324, 0.481

[a]Euler angles calculated with respect to the 2K61 CaM structure.

MO(R) represents the maximum percentage of time that the corresponding orientation can exist in any conformational ensemble (Bertini et al., 2010). The MO(R) values that have been calculated from these anisotropy and mean tensors by sampling all possible interdomain orientations are shown in Figure S5. It was found that all orientations have a MO larger than 0.17 and that no orientation can have a MO larger than 0.38. This means that rdc data alone do not indicate that any conformation can be excluded from the conformational ensemble sampled by the protein, independently of the corresponding interdomain orientation, although the maximum weight is different depending on the interdomain orientation and can vary from 0.17 to 0.38. The fact that even the interdomain orientations with largest MO(R) cannot have a weight larger than 0.38 confirms that extensive conformational averaging is indeed present.

Interestingly, the 10% interdomain orientations with largest MO(R) (above 0.325) are all similar to three representative orientations (Figure S5). These orientations were used as starting points to obtain the conformations, defined by orientation plus translation, with the largest MO. Therefore, pcs values of the C-terminal domain were introduced in the analysis, as well as the constraint on the maximum distance between residue 78 in the N-terminal domain and residue 81 in the C-terminal domain, which cannot exceed that given by the fully extended conformation of the intervening residues. The protocols determined the MO values of the conformations with the largest MO, portrayed in Figure 3D, corresponding to 0.31, 0.38, and 0.36. Figure 3C shows the plots reporting the minimum target function (TF) allowed by the experimental data as a function of the weight of such conformations. The MO is actually defined as the maximum weight of the conformation before the TF increases above the defined threshold. Figure 3C shows that independently of the exact positioning of the threshold and of the slight "fluctuations" in the minimization procedure, the MO of the conformation "a" is somewhat smaller than the MO of conformations "b" and "c," and that conformation "b" has a slightly larger MO than conformation "c." The agreement between calculated and experimental pcs values for the C-terminal domain amide protons is shown in Figure S3. Therefore, the conformations with the largest MO values are two of the three solutions with largest MO(R), with a MO of about 0.37. Other conformations will also be possible, with a smaller MO (see below). The real weight of all conformations can take any value in the range from zero to MO.

The conformational variability possibly experienced by CaM was then investigated through the calculation of the MO values for 430 CaM conformations randomly generated as representatives of all possible CaM conformations (Bertini et al., 2010). The indetermination of the MO values can be estimated ±0.01, as can be determined after multiple calculations performed for the same conformation using subsets of data, obtained after randomly removing 25% of the data. The results provide the map of MO values shown in Figure 4A. The position of the C-terminal domain of CaM is indicated by an orientation tensor centered on the center of mass of the C-terminal domain, color coded with respect to the MO of the corresponding conformation from blue (MO lower than 0.15) to red (MO greater than 0.35). Different orientations of the tensor reflect different orientations of the CaM C-terminal domain with respect to the N-terminal domain. The conformations having the C-terminal domain in the lower-right quadrant of the frame in Figure 4A have quite low MO values in general; the conformations having the C-terminal domain in the left quadrant of the frame in Figure 4A have also a relatively low MO, with some exceptions, which include conformation "a" of Figure 3D, with a relatively high MO. The conformations with higher MO are clustered in the central part of the distribution, corresponding to relatively elongated conformations, similarly to the results obtained for free CaM (Dasgupta et al., 2011). Conformations "b" and "c" of Figure 3D, those with largest MO, together with few other conformations with similar MO, are located on the right side of the central part of the distribution.

The persistence of a relatively extended conformation of CaM after binding of the MBP peptide was further supported on the basis of gel filtration chromatography (Figure S2), showing that the peptide did not increase significantly the compactness of CaM. Similar extended conformations for CaM upon recognition of target peptides have been also recently reported (Köster et al., 2011). These results are compatible with the previously determined radius of gyration of the complex of an MBP peptide with CaM (Majava et al., 2008), signifying an extended conformation of the relevant complex in solution. In addition, CD spectroscopy was used to monitor potential changes in the secondary structure components of CaM upon interaction with the MBP peptide (Figure S1). Again, it was further verified that the peptide does not alter the secondary structure of the CaM protein. The observed minor changes in the CaM spectrum can be attributed to the shift in the peptide structure that was shown to have high propensity for α-helical conformation.

Figure 4A also shows the MO values for the conformations of CaM that were found having the largest MO when the protein is free in solution (tensors circled with a purple dotted line) or interacting with the protein α-synuclein (tensor circled with a pink dotted line) (Bertini et al., 2007). In presence of the $MBP_{145–165}$ peptide, all these conformations have a relatively low MO value.

In conclusion, CaM can adopt a large ensemble of conformations while in complex with the $MBP_{145–165}$, similar to what is observed for the protein when free in solution and in the frame of CaM recognition by another IDP, α-synuclein. However, the

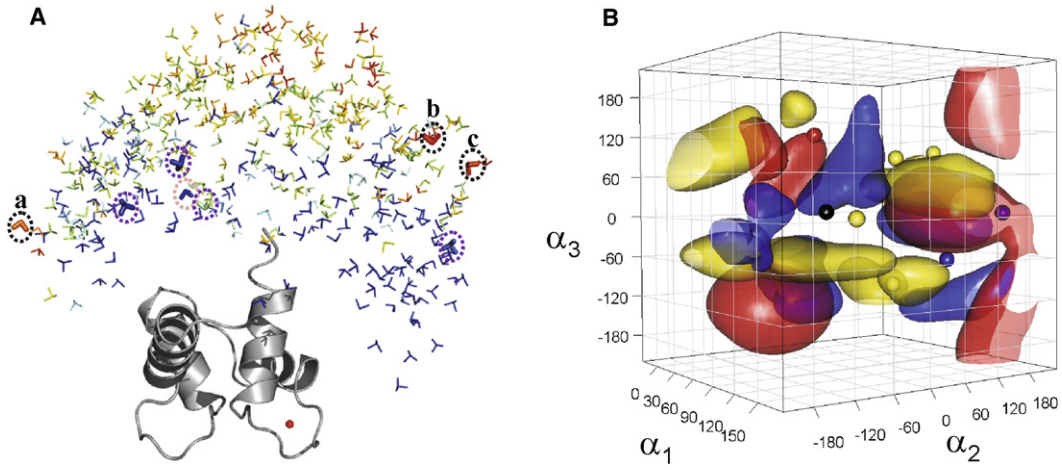

Figure 4. MO Analysis of CaM Conformations upon Binding to $MBP_{145–165}$ and Other Partners

(A) Arbitrary orientation tensors centered in the center of mass of the C-terminal domain, color coded with respect to the MO of the corresponding conformation from blue (lower than 0.15) to red (greater than 0.35) for 430 structures generated randomly with RANCH. Bold tensors circled with a black dotted line indicate the CaM conformations reported in Figure 3D as conformations a, b, and c; bold tensors circled with a purple or pink dotted line indicate the CaM conformations with largest MO calculated for the free protein or for the CaM-α-synuclein complex, respectively.

(B) Regions in the α_1, α_2, α_3 space (see text) with largest MO(R) in free CaM (yellow), in its adduct with α-synuclein (red) and with $MBP_{145–165}$ (blue). The small spheres represent the conformations with largest MO. The black sphere represents the conformation of CaM in its adduct with the DAPk peptide.

See also Figures S4 and S5.

conformations with the largest MO in the latter cases are different from those determined while in complex with the $MBP_{145–165}$.

Comparison of the Structural Heterogeneity of the CaM-$MBP_{145–165}$ Complex with Other CaM-Target Complexes and Free CaM

The structural heterogeneity revealed in the $MBP_{145–165}$-CaM complex could be a prerequisite for recognition pliability both for CaM and the MBP epitope. However, an emerging question is whether this mapped heterogeneity could be spatially conserved in other CaM complexes. Having a collective view of the largest MO values sampled by free CaM (Bertini et al., 2004), a rigid CaM-DAPk peptide complex (Bertini et al., 2009), the CaM-α-synuclein complex (Bertini et al., 2007), and the CaM-$MBP_{145–165}$ complex presented here, we performed a quantitative global comparative analysis of recognition heterogeneity induced in CaM upon interaction with different targets.

In order to quantify the potential structural heterogeneity consensus of CaM-target recognition, the Euler angles defining the relative orientations of the N-terminal and C-terminal domains of CaM were translated into three interdomain angles. The angle α_1 was defined to provide the interhelical angle between the last helix belonging to the N-terminal domain (IV CaM helix), and the first helix belonging to the C-terminal domain (V CaM helix). This angle is about 60° in the closed structure of CaM, as seen in the adduct with the DAPk peptide, for instance. The angle α_2 was defined referring to the projection of the first helix of the C-terminal domain in the plane perpendicular to the last helix of the N-terminal domain, with respect to the projection of the same helix observed in the case of the closed CaM structure. This angle thus indicates in which direction the first helix of the C-terminal domain is turned with respect to the N-terminal domain frame, and it is zero in the closed CaM structures. A third angle α_3 is defined to indicate the rotation of the C-terminal domain around its first helix, already positioned by the previously defined angles with respect to the N-terminal domain. This angle is defined in such a way as to be zero in the closed CaM structure. The α_1, α_2, and α_3 angles of the conformations corresponding to the largest MO values are shown as a 3D plot in Figure 4B. The plot, showing the regions with favored α_1, α_2, and α_3 angles for the three cases, indicates that a couple of zones are common to the different systems ($45° < \alpha_1 < 120°$, $-120° < \alpha_2 < -30°$, and $-120° < \alpha_3 < -60°$; $90° < \alpha_1 < 140°$, $60° < \alpha_2 < 180°$, and $-30° < \alpha_3 < 30°$), whereas other zones characterize each of them, and that the conformations with largest MO, although not clustered together, are restricted in the region defined by $60° < \alpha_1 < 140°$, $-30° < \alpha_2 < 180°$, and $-100° < \alpha_3 < 100°$. This comparative analysis indicates that distinct realms of spatial heterogeneity are sampled by the different CaM-target complexes.

To measure the degree of this spatial discreteness, we next mapped the similarity network of the CaM structures with largest MO. In the similarity network, each CaM structure, whether free or in complex with a partner, is represented as a node (Figure 5A). The nodes are connected if structures have a Cα rmsd below a defined cutoff (25 or 40 Å), and the Cα rmsd is used as a weight to determine the length of the edge (for more details see Supplemental Experimental Procedures). For a system that samples conformational space in a discrete manner, one expects the similarity network to consist of groups of structures (clusters) that are more similar among themselves than to any other structure in the network. Indeed, the similarity network reveals a consistent clustering of different CaM structures, independent of the cutoff used. A big cluster consists of all structures in which CaM binds targets in the classic "wrap-around" mode. A second

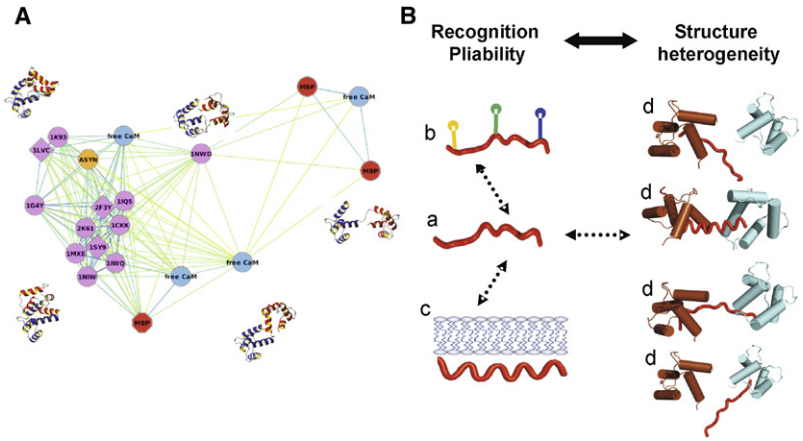

Figure 5. Functional Coupling in Protein Complexes of Structure Heterogeneity and Recognition Pliability

(A) Edge-weighted spring-embedded layout of the CaM structure-similarity network. Different structures of CaM (the nodes) are connected (the edges) if they have a Cα rmsd below 40 Å. The structures of unbound CaM, CaM when bound to MBP, α-synuclein, and any other target are represented by blue, red, orange, and magenta nodes, respectively. If the target proteins are highly structured (<25% of the residues predicted to be unstructured; prediction with DISOPRED2), moderately unstructured (25%–50% of the residues predicted to be unstructured), or highly unstructured (>50% of the residues predicted to be unstructured), the corresponding nodes have the shape of a diamond, sphere, or octagon, respectively. Clusters of structures that are more similar to themselves than to other structures in the network, and therefore detached from them (as a result of using the edge-weighted spring-embedded layout algorithm), are surrounded by dashed lines. Representative structures for each cluster are shown. See also Supplemental Experimental Procedures.

(B) Functional coupling in protein complexes of structure heterogeneity and recognition pliability. The disordered region 145–165 of MBP is indicated as a red random coiled structure (a). This region is implicated in recognition promiscuity because it can be recognized by numerous modifying enzymes (citrullination, serine, and threonine phosphorylation) (b), it can associate with membrane accompanied with a structural transition to an amphipathic α helix (c), and it can be recognized by CaM (d). The N and C terminus lobes of CaM are indicated in brown and cyan respectively, whereas the MBP-derived peptide is indicated as a red solid line. This recognition promiscuity could be assisted by structural heterogeneity as determined for the MBP145–165-CaM complex.

cluster contains the structures that have revealed a more open binding mode of CaM (1K93, 1G4Y, and 1LVC). This cluster also contains α-synuclein. Most importantly, structures of CaM when bound to $MBP_{145–165}$ lie in independent and distinct clusters that harbor different structures of unbound CaM. It is interesting to note that the structure in which CaM binds a dimeric helical target (1NWD) does not belong to any cluster. The CaM structure-similarity network reinforces the concept of a discrete spatial heterogeneity in CaM sampling and reveals its topology.

Conclusions

Here, we focused on a largely disordered binding region of MBP that is functionally versatile because it is involved in binding to CaM, is targeted by modifying enzymes, and associates with membranes and cytoskeletal proteins. CaM orchestrates key roles in numerous signaling pathways through its ability to bind a wide range of targets (Crivici and Ikura, 1995; Hoeflich and Ikura, 2002; Yap et al., 2000). It has been suggested that CaM recognizes IDP regions (Radivojac et al., 2006), but the conformational space sampled by such complexes is not fully documented. Here, we found that CaM can adopt a large ensemble of conformations when in complex with the segment $MBP_{145–165}$. This flexibility in the CaM-$MBP_{145–165}$ complex could provide a potential basis for the explanation of the functional diversity associated by this disordered region. The ability of such complexes to assume many different shapes could be involved in fine-tuning the functioning (and malfunctioning) of their disordered protein partner. Indeed, such disordered complexes could monitor the motional degree between domains, allow overlapping binding motifs through transient binding of different binding partners, mask binding sites, and be targets of posttranslational modifications, thus enabling signal decoding through this plasticity.

Our studies provide insight into the heterogeneity and the conformational space sampled by the complex of CaM and an IDP-binding region $MBP_{145–165}$. MOs of multiple conformations sampled by this complex were determined on the basis of simultaneous use of paramagnetic pcs and rdc restraints. The complex CaM-$MBP_{145–165}$ confers conformational heterogeneity, which differs from other CaM complexes, to provide the plasticity necessary to interact with a large number of different targets. The recorded disorder in this complex could provide an additional understanding of how IDP-binding regions transmit and realize their multiple functions within complexes. Functional coupling of structural heterogeneity and recognition pliability in protein complexes could be envisioned as a mechanism enabling the fine-tuning a system's response to various cellular events (Figure 5B). Because disordered complexes are prone to make promiscuous molecular contacts that can cause pathology (Uversky, 2010; Uversky et al., 2008; Vavouri et al., 2009), new approaches to discover drug molecules that target IDP-binding regions are a high priority (Iakoucheva et al., 2002; Janga and Tzakos, 2009; Uversky et al., 2009). We suggest that such disorder information within the complex level should be employed in the future to develop new strategies for the discovery of new drugs.

EXPERIMENTAL PROCEDURES

Solid-Phase Peptide Synthesis of the Linear $MBP_{145–165}$ Peptide

The linear-protected peptide was prepared on the acid-sensitive 2-chlorotrityl chloride resin (CLTR-Cl) using Fmoc/tBu methodology (details can be found in the Supplemental Experimental Procedures). Peptide purity was assessed by analytical reverse-phase high-performance liquid chromatography (RP-HPLC), thin-layer chromatography (TLC) (BAW, 4:1:1), and electrospray ionization mass spectrometry (ESI-MS).

CD Spectroscopy

Samples of pure $MBP_{145–165}$ were prepared by dissolving the peptides in different mixtures of distilled water and TFE, resulting in $MBP_{145–165}$ concentrations of 55 μM. The CD spectra of this hydrophobicity series were recorded on a Jasco J-810 spectropolarimeter (Jasco International, Tokyo) using

a 1 mm path length cell, 0.5 nm data pitch, 0.25 s response time, 20 nm/min scan speed, 1 nm bandwidth, and ten scans. Next, model membranes of either pure DMPC or a DMPC/DMPG mixture (3:1 molar ratio) were prepared by solubilizing the appropriate amount of lipid in methanol/chloroform (1/1, v/v), followed by removal of the organic solvents with a flow of nitrogen gas, and the addition of 600 μl of distilled water. This suspension was sonicated (2 min, 25% duty cycle, input power of 40 W, Branson 250 tip sonicator) to obtain unilamellar vesicles, and centrifuged (5 min, 12,000 × *g*) to pellet down the titanium particles and any residual multilamellar structures. A concentrated peptide solution in distilled water (30 μl) was added to the clear supernatant fraction of sonicated vesicles (400 μl), resulting in samples with a concentration of 50 μM of $MBP_{145–165}$, with a peptide/lipid molar ratio of 1:20. The CD spectra were recorded as described, except with a longer response time of 0.5 s. To obtain aligned multilayers, 200 μl of selected peptide/lipid samples was spread out on the side of a quartz cuvette, and the excess water was removed with a nitrogen flow. Oriented CD spectra were recorded (1.0 s response time, 20 scans) to assess the peptide topology (de Planque et al., 1999). All spectra were corrected for the contribution of the lipids and smoothed. In addition, CD measurements were also carried out in 20 mM HEPES/150 mM NaCl (pH 7.4) using 120 μM of Ca_4CaM in the presence or absence of 300 μM MBP peptide.

ITC

ITC experiments were carried out using a VP-ITC instrument from MicroCal (Northampton, MA, USA). Lyophilized apo-calmodulin (apoCaM) was dissolved in 20 mM HEPES/150 mM NaCl/20 mM $CaCl_2$ (pH 7.4) and was then extensively dialyzed in 20 mM HEPES/150 mM NaCl (pH 7.4) (at least four changes). In addition to the Ca_4CaM protein, a sample of Ca_3TmCaM was also prepared for ITC. Following the dialysis the protein was filtered (0.22 μm), and the concentration was estimated from the absorbance at 276 nm = 1.97 (1%, 1 cm). MBP peptide was dissolved in the same solution (20 mM HEPES/150 mM NaCl [pH 7.4]) prior to experiment. Samples were degassed in a ThermoVac (Northampton, MA) at 24°C for 10 min. The MBP peptide solution (1.0 mM) was injected into the sample cell, containing 0.10 mM CaM in the aforementioned solution. Typically, the titrations were carried out with a preliminary injection of 2 μl followed by 47 injections of 6 μl of peptide solution with 300 s spacing between each. All experiments were carried out at 25°C. Before analysis, data from the preliminary 2 μl injection were discarded, and heats of dilution of the peptide into solution of 20 mM HEPES/150 mM NaCl (pH 7.4) (in the absence of CaM) were subtracted from the peptide into CaM experiments. The corrected data were integrated and plotted as a function of the molar ratio, and the binding isotherms obtained were fitted to the Origin "one set of sites" and "sequential binding sets" models (Origin 5.0; MicroCal) (Majava et al., 2008).

NMR Sample Preparation

The ^{15}N- and ^{13}C-labeled N60D CaM was purchased from ProtEra (Florence, Italy; http://www.proterasrl.com). Samples of Ca_4CaM and $LnCa_3CaM$ (Ln = Tb, Tm, and Dy) were prepared as previously reported (Bertini et al., 2010), in solution with 150 mM NaCl, 20 mM HEPES (pH 7.4) for NMR spectroscopy studies. The N60D CaM variant was used because the lanthanide ions were previously proven to selectively bind this protein in the second calcium binding loop of the N-terminal domain (Bertini et al., 2003). The lanthanide binding to the protein was monitored by following the changes in the ^1H-^{15}N HSQC NMR spectrum during metal titration. The presence of a single peak for the backbone HN nuclei of any protein residue ensures that the lanthanides bind in a single site. This is also supported by the fact that the peaks of each residue in the Ca_4CaM and the $LnCa_3CaM$ (Ln = Tb, Tm, and Dy) samples are along a diagonal line, as predicted by theory in the presence of a single binding site.

NMR Experiments

The ^1H-^{15}N HSQC experiments were performed at 700 MHz, 298 K. The CaM concentration was around 0.5 mM. The pcs data were obtained as the ^1H chemical shift difference between the paramagnetic form (terbium, thulium, or dysprosium) and the diamagnetic (calcium) form of CaM in the presence of $MBP_{145–165}$. The HN rdc data were obtained from IPAP experiments at 700 MHz as the difference in the doublet splitting in the indirect ^{15}N dimension between the paramagnetic form and the diamagnetic form.

NMR Analysis of the Paramagnetic Data and MO Calculations

The pcs values of N-terminal domain amide protons of CaM were fit to the CaM structure calculated in the adduct with the DAPk peptide (see later) using Equation 1:

$$\Delta\delta^{pcs} = \frac{1}{12\pi r^3}\left[\Delta\chi_{ax}\left(3\cos^2\theta - 1\right) + \frac{3}{2}\Delta\chi_{rh}\sin^2\theta\cos 2\phi\right], \quad \text{(Equation 1)}$$

where r is the distance between the observed nuclei and the metal ion, θ and ϕ denote the polar coordinates of the nucleus in the frame of the magnetic susceptibility tensor, and $\Delta\chi_{ax}$ and $\Delta\chi_{rh}$ are the axial and rhombic anisotropy parameters of the magnetic susceptibility tensor of the metal. The good quality of the fit of the pcs of the N-terminal domain (shown in Figure S5) to the N-terminal domain structure of CaM indicates that lanthanide substitution is not responsible for any sizable change in the structural arrangement of the protein.

The ^{H}H-N rdc values of the C-terminal domain of CaM were fit to the rdc-refined CaM structures when free in solution and when bound to the DAPk peptide. The agreement between experimental and calculated values was higher when the structure calculated in the adduct with the DAPk peptide was used, so that structure was chosen for all subsequent calculations. The fit to Equation 2 provided the mean tensor parameters (reported in Table 1) for the three lanthanides:

$$rdc(\mathrm{Hz}) = -\frac{1}{4\pi}\frac{B_0^2}{15kT}\frac{\gamma_N\gamma_H\hbar}{2\pi r_{HN}^3}\left[\Delta\chi_{ax}\left(3\cos^2\theta - 1\right) + \frac{3}{2}\Delta\chi_{rh}\sin^2\Theta\cos 2\Phi\right], \quad \text{(Equation 2)}$$

where r_{HN} is the distance between the two coupled nuclei N and ^{N}H, and the polar angles Θ and Φ are those defining the orientation of the vector connecting the coupled nuclei in the frame of the magnetic susceptibility tensor. Other symbols have the usual meaning. In the case of a rigid protein structure, the $\Delta\chi_{ax}$ and $\Delta\chi_{rh}$ values obtained from Equation 1 and Equation 2 must coincide.

MO(R) and MO values were calculated according to the programs presented in Bertini et al. (2007, 2010) and Dasgupta et al. (2011). MO(R) is the MO for a specific interdomain orientation, as determined using rdc data alone. It is calculated using a geometric algorithm without the requirement of heavy minimization procedures due to the mathematical properties of the rdc restraints. MO is the maximum allowed probability for a specific protein conformation and, thus, depends on the interdomain position, i.e., on both the relative orientational and translational parameters, and it is determined from pcs and rdc (and possibly paramagnetic relaxation enhancements and small-angle scattering [SAS]) restraints. The MO of each conformation X_0 is calculated by searching for ensembles of conformations that comprise the conformation X_0, with weights chosen in order to have the maximum allowed weight for the conformation X_0, and providing averaged pcs and rdc values in agreement with all the experimental restraints. This is performed by applying a simulated annealing minimization procedure for each selected conformation X_0 complemented by other N = *9* conformations, with weight (w_i), position (t_i), and orientation (R_i) obtained in order to minimize the TF:

$$TF(w_\circ) = \min_{t_0,\{w_i,t_i,R_i\}}\sum_j\left|\tilde{\delta}_j - \left(w_0\delta_j(t_0,R_0) + \sum_{i=1}^{n} w_i\delta_j(t_i,R_i)\right)\right|^2, \quad \text{(Equation 3)}$$

where $\tilde{\delta}_j$ are the experimental pcs/rdc values, $\delta_j(t_0,R_0)$ are the pcs/rdc values calculated for the selected conformation X_0 with orientation R_0, with the translation vector t_0 defining its position, w_0 is the corresponding weight, and $\delta_j(t_i,R_i)$ are the pcs/rdc values calculated for the other $i = 1\ldots N$ conformations. Such a function (with $w_0 + \sum w_i = 1$) represents the minimal error on the reconstructed data when the domain is constrained to stay in orientation R_0 for a fraction w_0 of the time. A weighting factor was introduced to normalize the contributions to the TF from pcss and from rdcs according to their squared values, and to make them of the same order. Once the best-fit conformations were found, they were fixed, and the function $TF(w_0)$ was calculated for increasing and decreasing values of w_0. This procedure, previously used for the analysis of the conformations with largest MO of CaM when free or complexed to α-synuclein, was developed to deal with the large number of parameters that make the minimization quite difficult. The MO value was then defined as the largest w_0 value such that $TF(w_0) = \varepsilon$, where ε is the threshold fixed for the error. This was set to a 10% larger value of the absolute

minimum of the *TF*. Calculations of the MO values were performed for 430 selected conformations (X_0), randomly generated as representatives of all possible CaM conformations. Similar calculations were also performed by allowing the orientation R_0 and the translation vector t_0 to locally change during the simulating annealing procedure around their initial values. This was performed to determine the conformations with largest MO.

Gel Filtration Chromatography

Gel filtration chromatography with the ÄKTA*explorer* system (GE Healthcare) was used to study the difference in the mobility of CaM in the presence and absence of the peptide. A Superdex 75 HR 10/30 column (GE Healthcare) with void volume (V_0) of 9,465 ml and total column volume (V_T) of 24,000 ml was equilibrated with 20 mM HEPES buffer (pH 7.4), 150 mM NaCl and calibrated with a mixture of proteins with known molecular weights (MWs). The experiments were run at a flow rate of 0.8 ml/min; the injection volumes were 250 μl, which contained 30 nmol of CaM in the presence or absence of 75 nmol of the peptide.

SUPPLEMENTAL INFORMATION

Supplemental Information includes five figures, four tables, and Supplemental Experimental Procedures and can be found with this article online at doi:10.1016/j.str.2012.01.021.

ACKNOWLEDGMENTS

We are grateful to Luca Sgheri, Zsuzsanna Dosztanyi, Nikolaos Papanikolaou, Sarath Janga, and Francesca Magnani for helpful discussions and suggestions, as well as an unknown reviewer for his or her insightful comments. Professor Predrag Radivojac is acknowledged for providing prediction of CaM-binding regions. This work has been supported by Ente Cassa di Risparmio di Firenze, MIUR-FIRB contracts RBLA032ZM7 and RBRN07BMCT, the Canadian Institutes of Health Research CIHR (MOP #74468 to G.H.), the Esthir-Gkani Foundation, and by the EC contracts EU-NMR n. 026145, WeNMR n. 261572, and Bio-NMR n. 261863. V.V.B. was the recipient of a postdoctoral fellowship from MSSC the Multiple Sclerosis Society of Canada. M.M.B. is an EMBO Young Investigator and acknowledges the Medical Research Council for funding his research. We are grateful to the National Strategic Reference Framework, Regional Operational Program of Epirus 2007-2013 (2011/S 29-048013), for supporting the purchase of an ITC200 instrument.

Received: July 15, 2011
Revised: December 1, 2011
Accepted: January 3, 2012
Published: March 6, 2012

REFERENCES

Abraham, S.J., Nolet, R.P., Calvert, R.J., Anderson, L.M., and Gaponenko, V. (2009). The hypervariable region of K-Ras4B is responsible for its specific interactions with calmodulin. Biochemistry *48*, 7575–7583.

Baber, J.L., Szabo, A., and Tjandra, N. (2001). Analysis of slow interdomain motion of macromolecules using NMR relaxation data. J. Am. Chem. Soc. *123*, 3953–3959.

Barbato, G., Ikura, M., Kay, L.E., Pastor, R.W., and Bax, A. (1992). Backbone dynamics of calmodulin studied by 15N relaxation using inverse detected two-dimensional NMR spectroscopy: the central helix is flexible. Biochemistry *31*, 5269–5278.

Bertini, I., Luchinat, C., and Parigi, G. (2002). Magnetic susceptibility in paramagnetic NMR. Prog. Nucl. Magn. Reson. Spectrosc. *40*, 249–273.

Bertini, I., Gelis, I., Katsaros, N., Luchinat, C., and Provenzani, A. (2003). Tuning the affinity for lanthanides of calcium binding proteins. Biochemistry *42*, 8011–8021.

Bertini, I., Del Bianco, C., Gelis, I., Katsaros, N., Luchinat, C., Parigi, G., Peana, M., Provenzani, A., and Zoroddu, M.A. (2004). Experimentally exploring the conformational space sampled by domain reorientation in calmodulin. Proc. Natl. Acad. Sci. USA *101*, 6841–6846.

Bertini, I., Luchinat, C., Parigi, G., and Pierattelli, R. (2005). NMR spectroscopy of paramagnetic metalloproteins. ChemBioChem *6*, 1536–1549.

Bertini, I., Gupta, Y.K., Luchinat, C., Parigi, G., Peana, M., Sgheri, L., and Yuan, J. (2007). Paramagnetism-based NMR restraints provide maximum allowed probabilities for the different conformations of partially independent protein domains. J. Am. Chem. Soc. *129*, 12786–12794.

Bertini, I., Kursula, P., Luchinat, C., Parigi, G., Vahokoski, J., Wilmanns, M., and Yuan, J. (2009). Accurate solution structures of proteins from X-ray data and a minimal set of NMR data: calmodulin-peptide complexes as examples. J. Am. Chem. Soc. *131*, 5134–5144.

Bertini, I., Giachetti, A., Luchinat, C., Parigi, G., Petoukhov, M.V., Pierattelli, R., Ravera, E., and Svergun, D.I. (2010). Conformational space of flexible biological macromolecules from average data. J. Am. Chem. Soc. *132*, 13553–13558.

Boehr, D.D., Nussinov, R., and Wright, P.E. (2009). The role of dynamic conformational ensembles in biomolecular recognition. Nat. Chem. Biol. *5*, 789–796.

Boggs, J.M. (2006). Myelin basic protein: a multifunctional protein. Cell. Mol. Life Sci. *63*, 1945–1961.

Boggs, J.M., and Rangaraj, G. (2000). Interaction of lipid-bound myelin basic protein with actin filaments and calmodulin. Biochemistry *39*, 7799–7806.

Boggs, J.M., Rangaraj, G., Heng, Y.M., Liu, Y., and Harauz, G. (2011). Myelin basic protein binds microtubules to a membrane surface and to actin filaments in vitro: effect of phosphorylation and deimination. Biochim. Biophys. Acta *1808*, 761–773.

Cheng, Y., LeGall, T., Oldfield, C.J., Mueller, J.P., Van, Y.Y., Romero, P., Cortese, M.S., Uversky, V.N., and Dunker, A.K. (2006). Rational drug design via intrinsically disordered protein. Trends Biotechnol. *24*, 435–442.

Crivici, A., and Ikura, M. (1995). Molecular and structural basis of target recognition by calmodulin. Annu. Rev. Biophys. Biomol. Struct. *24*, 85–116.

Csermely, P., Palotai, R., and Nussinov, R. (2010). Induced fit, conformational selection and independent dynamic segments: an extended view of binding events. Trends Biochem. Sci. *35*, 539–546.

Csermely, P., Sandhu, K.S., Hazai, E., Hoksza, Z., Kiss, H.J., Veres, D.V., Piazza, F., and Nussinov, R. (2011). Disordered proteins and network disorder in network descriptions of protein structure, dynamics and function. Hypotheses and a comprehensive review. Curr. Protein Pept. Sci. Published online October 25, 2011.

Dasgupta, S., Hu, X., Keizers, P.H., Liu, W.M., Luchinat, C., Nagulapalli, M., Overhand, M., Parigi, G., Sgheri, L., and Ubbink, M. (2011). Narrowing the conformational space sampled by two-domain proteins with paramagnetic probes in both domains. J. Biomol. NMR *51*, 253–263.

de Planque, M.R., Kruijtzer, J.A., Liskamp, R.M., Marsh, D., Greathouse, D.V., Koeppe, R.E., 2nd, de Kruijff, B., and Killian, J.A. (1999). Different membrane anchoring positions of tryptophan and lysine in synthetic transmembrane α-helical peptides. J. Biol. Chem. *274*, 20839–20846.

Deraos, G., Chatzantoni, K., Matsoukas, M.T., Tselios, T., Deraos, S., Katsara, M., Papathanasopoulos, P., Vynios, D., Apostolopoulos, V., Mouzaki, A., and Matsoukas, J. (2008). Citrullination of linear and cyclic altered peptide ligands from myelin basic protein (MBP(87-99)) epitope elicits a Th1 polarized response by T cells isolated from multiple sclerosis patients: implications in triggering disease. J. Med. Chem. *51*, 7834–7842.

Dunker, A.K., Oldfield, C.J., Meng, J., Romero, P., Yang, J.Y., Chen, J.W., Vacic, V., Obradovic, Z., and Uversky, V.N. (2008). The unfoldomics decade: an update on intrinsically disordered proteins. BMC Genomics *9* (*Suppl 2*), S1.

Dyson, H.J., and Wright, P.E. (2002). Coupling of folding and binding for unstructured proteins. Curr. Opin. Struct. Biol. *12*, 54–60.

Elshorst, B., Hennig, M., Försterling, H., Diener, A., Maurer, M., Schulte, P., Schwalbe, H., Griesinger, C., Krebs, J., Schmid, H., et al. (1999). NMR solution structure of a complex of calmodulin with a binding peptide of the Ca2+ pump. Biochemistry *38*, 12320–12332.

Fong, J.H., Shoemaker, B.A., Garbuzynskiy, S.O., Lobanov, M.Y., Galzitskaya, O.V., and Panchenko, A.R. (2009). Intrinsic disorder in protein interactions: insights from a comprehensive structural analysis. PLoS Comput. Biol. *5*, e1000316.

Gsponer, J., Futschik, M.E., Teichmann, S.A., and Babu, M.M. (2008). Tight regulation of unstructured proteins: from transcript synthesis to protein degradation. Science *322*, 1365–1368.

Hammoudeh, D.I., Follis, A.V., Prochownik, E.V., and Metallo, S.J. (2009). Multiple independent binding sites for small-molecule inhibitors on the oncoprotein c-Myc. J. Am. Chem. Soc. *131*, 7390–7401.

Harauz, G., and Libich, D.S. (2009). The classic basic protein of myelin—conserved structural motifs and the dynamic molecular barcode involved in membrane adhesion and protein-protein interactions. Curr. Protein Pept. Sci. *10*, 196–215.

Hoeflich, K.P., and Ikura, M. (2002). Calmodulin in action: diversity in target recognition and activation mechanisms. Cell *108*, 739–742.

Homchaudhuri, L., De Avila, M., Nilsson, S.B., Bessonov, K., Smith, G.S., Bamm, V.V., Musse, A.A., Harauz, G., and Boggs, J.M. (2010). Secondary structure and solvent accessibility of a calmodulin-binding C-terminal segment of membrane-associated myelin basic protein. Biochemistry *49*, 8955–8966.

Iakoucheva, L.M., Brown, C.J., Lawson, J.D., Obradović, Z., and Dunker, A.K. (2002). Intrinsic disorder in cell-signaling and cancer-associated proteins. J. Mol. Biol. *323*, 573–584.

Ishida, H., and Vogel, H.J. (2006). Protein-peptide interaction studies demonstrate the versatility of calmodulin target protein binding. Protein Pept. Lett. *13*, 455–465.

Ishiyama, N., Bates, I.R., Hill, C.M., Wood, D.D., Matharu, P., Viner, N.J., Moscarello, M.A., and Harauz, G. (2001). The effects of deimination of myelin basic protein on structures formed by its interaction with phosphoinositide-containing lipid monolayers. J. Struct. Biol. *136*, 30–45.

Janga, S.C., and Tzakos, A. (2009). Structure and organization of drug-target networks: insights from genomic approaches for drug discovery. Mol. Biosyst. *5*, 1536–1548.

Juranic, N., Atanasova, E., Filoteo, A.G., Macura, S., Prendergast, F.G., Penniston, J.T., and Strehler, E.E. (2010). Calmodulin wraps around its binding domain in the plasma membrane Ca2+ pump anchored by a novel 18-1 motif. J. Biol. Chem. *285*, 4015–4024.

Katsara, M., Yuriev, E., Ramsland, P.A., Tselios, T., Deraos, G., Lourbopoulos, A., Grigoriadis, N., Matsoukas, J., and Apostolopoulos, V. (2009). Altered peptide ligands of myelin basic protein (MBP87-99) conjugated to reduced mannan modulate immune responses in mice. Immunology *128*, 521–533.

Köster, S., Pavkov-Keller, T., Kühlbrandt, W., and Yildiz, Ö. (2011). Structure of human Na+/H+ exchanger NHE1 regulatory region in complex with calmodulin and Ca2+. J. Biol. Chem. *286*, 40954–40961.

Libich, D.S., and Harauz, G. (2008). Backbone dynamics of the 18.5 kDa isoform of myelin basic protein reveals transient alpha-helices and a calmodulin-binding site. Biophys. J. *94*, 4847–4866.

Libich, D.S., Hill, C.M., Bates, I.R., Hallett, F.R., Armstrong, S., Siemiarczuk, A., and Harauz, G. (2003a). Interaction of the 18.5-kD isoform of myelin basic protein with Ca2+ -calmodulin: effects of deimination assessed by intrinsic Trp fluorescence spectroscopy, dynamic light scattering, and circular dichroism. Protein Sci. *12*, 1507–1521.

Libich, D.S., Hill, C.M., Haines, J.D., and Harauz, G. (2003b). Myelin basic protein has multiple calmodulin-binding sites. Biochem. Biophys. Res. Commun. *308*, 313–319.

Libich, D.S., Ahmed, M.A., Zhong, L., Bamm, V.V., Ladizhansky, V., and Harauz, G. (2010). Fuzzy complexes of myelin basic protein: NMR spectroscopic investigations of a polymorphic organizational linker of the central nervous system. Biochem. Cell Biol. *88*, 143–155.

Majava, V., Petoukhov, M.V., Hayashi, N., Pirilä, P., Svergun, D.I., and Kursula, P. (2008). Interaction between the C-terminal region of human myelin basic protein and calmodulin: analysis of complex formation and solution structure. BMC Struct. Biol. *8*, 10.

Majava, V., Wang, C., Myllykoski, M., Kangas, S.M., Kang, S.U., Hayashi, N., Baumgartel, P., Heape, A.M., Lubec, G., and Kursula, P. (2010). Structural analysis of the complex between calmodulin and full-length myelin basic protein, an intrinsically disordered molecule. Amino Acids *39*, 59–71.

Matsoukas, J., Apostolopoulos, V., Kalbacher, H., Papini, A.M., Tselios, T., Chatzantoni, K., Biagioli, T., Lolli, F., Deraos, S., Papathanassopoulos, P., et al. (2005). Design and synthesis of a novel potent myelin basic protein epitope 87-99 cyclic analogue: enhanced stability and biological properties of mimics render them a potentially new class of immunomodulators. J. Med. Chem. *48*, 1470–1480.

Mészáros, B., Simon, I., and Dosztányi, Z. (2009). Prediction of protein binding regions in disordered proteins. PLoS Comput. Biol. *5*, e1000376.

Metallo, S.J. (2010). Intrinsically disordered proteins are potential drug targets. Curr. Opin. Chem. Biol. *14*, 481–488.

Mittag, T., Kay, L.E., and Forman-Kay, J.D. (2010). Protein dynamics and conformational disorder in molecular recognition. J. Mol. Recognit. *23*, 105–116.

Oldfield, C.J., Meng, J., Yang, J.Y., Yang, M.Q., Uversky, V.N., and Dunker, A.K. (2008). Flexible nets: disorder and induced fit in the associations of p53 and 14-3-3 with their partners. BMC Genomics *9* (*Suppl 1*), S1.

Polverini, E., Boggs, J.M., Bates, I.R., Harauz, G., and Cavatorta, P. (2004). Electron paramagnetic resonance spectroscopy and molecular modelling of the interaction of myelin basic protein (MBP) with calmodulin (CaM)-diversity and conformational adaptability of MBP CaM-targets. J. Struct. Biol. *148*, 353–369.

Radivojac, P., Vucetic, S., O'Connor, T.R., Uversky, V.N., Obradovic, Z., and Dunker, A.K. (2006). Calmodulin signaling: analysis and prediction of a disorder-dependent molecular recognition. Proteins *63*, 398–410.

Receveur-Bréchot, V., Bourhis, J.M., Uversky, V.N., Canard, B., and Longhi, S. (2006). Assessing protein disorder and induced folding. Proteins *62*, 24–45.

Rhoads, A.R., and Friedberg, F. (1997). Sequence motifs for calmodulin recognition. FASEB J. *11*, 331–340.

Rodríguez-Castañeda, F., Maestre-Martínez, M., Coudevylle, N., Dimova, K., Junge, H., Lipstein, N., Lee, D., Becker, S., Brose, N., Jahn, O., et al. (2010). Modular architecture of Munc13/calmodulin complexes: dual regulation by Ca2+ and possible function in short-term synaptic plasticity. EMBO J. *29*, 680–691.

Romero, P., Obradovic, Z., Li, X., Garner, E.C., Brown, C.J., and Dunker, A.K. (2001). Sequence complexity of disordered protein. Proteins *42*, 38–48.

Samal, A.B., Ghanam, R.H., Fernandez, T.F., Monroe, E.B., and Saad, J.S. (2011). NMR, biophysical, and biochemical studies reveal the minimal Calmodulin binding domain of the HIV-1 matrix protein. J. Biol. Chem. *286*, 33533–33543.

Singh, D., Tangirala, R., Bakthisaran, R., and Chintalagiri, M.R. (2009). Synergistic effects of metal ion and the pre-senile cataract-causing G98R alphaA-crystallin: self-aggregation propensities and chaperone activity. Mol. Vis. *15*, 2050–2060.

Sospedra, M., and Martin, R. (2005). Immunology of multiple sclerosis. Annu. Rev. Immunol. *23*, 683–747.

Sugase, K., Dyson, H.J., and Wright, P.E. (2007). Mechanism of coupled folding and binding of an intrinsically disordered protein. Nature *447*, 1021–1025.

Tarassov, K., Messier, V., Landry, C.R., Radinovic, S., Serna Molina, M.M., Shames, I., Malitskaya, Y., Vogel, J., Bussey, H., and Michnick, S.W. (2008). An in vivo map of the yeast protein interactome. Science *320*, 1465–1470.

Tokuriki, N., and Tawfik, D.S. (2009). Protein dynamism and evolvability. Science *324*, 203–207.

Tompa, P., and Fuxreiter, M. (2008). Fuzzy complexes: polymorphism and structural disorder in protein-protein interactions. Trends Biochem. Sci. *33*, 2–8.

Turoverov, K.K., Kuznetsova, I.M., and Uversky, V.N. (2010). The protein kingdom extended: ordered and intrinsically disordered proteins, their folding, supramolecular complex formation, and aggregation. Prog. Biophys. Mol. Biol. *102*, 73–84.

Tzakos, A.G., Fuchs, P., van Nuland, N.A., Troganis, A., Tselios, T., Deraos, S., Matsoukas, J., Gerothanassis, I.P., and Bonvin, A.M. (2004). NMR and

molecular dynamics studies of an autoimmune myelin basic protein peptide and its antagonist: structural implications for the MHC II (I-Au)-peptide complex from docking calculations. Eur. J. Biochem. *271*, 3399–3413.

Uversky, V.N. (2010). Targeting intrinsically disordered proteins in neurodegenerative and protein dysfunction diseases: another illustration of the D(2) concept. Expert Rev. Proteomics *7*, 543–564.

Uversky, V.N., Oldfield, C.J., and Dunker, A.K. (2008). Intrinsically disordered proteins in human diseases: introducing the D2 concept. Annu. Rev. Biophys. *37*, 215–246.

Uversky, V.N., Oldfield, C.J., Midic, U., Xie, H., Xue, B., Vucetic, S., Iakoucheva, L.M., Obradovic, Z., and Dunker, A.K. (2009). Unfoldomics of human diseases: linking protein intrinsic disorder with diseases. BMC Genomics *10* (*Suppl 1*), S7.

Vavouri, T., Semple, J.I., Garcia-Verdugo, R., and Lehner, B. (2009). Intrinsic protein disorder and interaction promiscuity are widely associated with dosage sensitivity. Cell *138*, 198–208.

Yamauchi, E., Nakatsu, T., Matsubara, M., Kato, H., and Taniguchi, H. (2003). Crystal structure of a MARCKS peptide containing the calmodulin-binding domain in complex with Ca2+-calmodulin. Nat. Struct. Biol. *10*, 226–231.

Yap, K.L., Kim, J., Truong, K., Sherman, M., Yuan, T., and Ikura, M. (2000). Calmodulin target database. J. Struct. Funct. Genomics *1*, 8–14.

Zhong, L., Bamm, V.V., Ahmed, M.A., Harauz, G., and Ladizhansky, V. (2007). Solid-state NMR spectroscopy of 18.5 kDa myelin basic protein reconstituted with lipid vesicles: spectroscopic characterisation and spectral assignments of solvent-exposed protein fragments. Biochim. Biophys. Acta *1768*, 3193–3205.